

# A Parsimonious Dynamical Model for Structural Learning in the Human Brain

Zhixin Lu<sup>1</sup>, Danielle S. Bassett<sup>1,2,3,4,5</sup>

<sup>1</sup>*Department of Bioengineering, School of Engineering and Applied Sciences, University of Pennsylvania, Philadelphia, PA, 19104*

<sup>2</sup>*Department of Physics & Astronomy, College of Arts and Sciences, University of Pennsylvania, Philadelphia, PA, 19104*

<sup>3</sup>*Department of Electrical and Systems Engineering, School of Engineering and Applied Sciences, University of Pennsylvania, Philadelphia, PA, 19104*

<sup>4</sup>*Department of Neurology, Perelman School of Medicine, University of Pennsylvania, Philadelphia, PA, 19104*

<sup>5</sup>*To whom correspondence should be addressed: dsb@seas.upenn.edu*

The human brain is capable of diverse feats of intelligence. A particularly salient example is the ability to deduce structure from time-varying auditory and visual stimuli, enabling humans to master the rules of language and to build rich expectations of their physical environment. The broad relevance of this ability for human cognition motivates the need for a first-principles model explicating putative mechanisms. Here we propose a general framework for structural learning in the brain, composed of an evolving, high-dimensional dynamical system driven by external stimuli or internal processes. We operationalize the scenario in which humans learn the rules that generate a sequence of stimuli, rather than the exemplar stimuli themselves. We model external stimuli as seemingly disordered chaotic time series generated by complex dynamical systems; the underlying structure being deduced is then that of the corresponding chaotic attractor. This approach allows us to demonstrate and theoretically explain the emergence of five distinct phenomena reminiscent of cognitive functions: (i) learning the structure of a chaotic system purely from time series, (ii) generating new streams of stimuli from a chaotic system, (iii) switching stream generation among multiple learned chaotic systems, either spontaneously or in response to external perturbations, (iv) inferring missing data from sparse observations of the chaotic system, and (v) deciphering superimposed input from different chaotic systems. Numerically, we show that these phenomena emerge naturally from a recurrent neural network of Erdős-Rényi topology in which the synaptic strengths adapt in a Hebbian-like manner. Broadly, our work blends chaotic theory and artificial neural networks to answer the long standing question of how neural systems can learn the structure underlying temporal sequences of stimuli.

The brain perpetually processes streams of time-varying sensory stimuli that bear different sorts of information. One type of information concerns the statistics of how objects, concepts, or other features are ordered or arranged in the stream, while another type of information concerns the structure underlying the stream, and the rules by which that structure is sampled to obtain the stream. In poetry, for example, the former type of information lies in the choice and arrangement of words, while the latter type of information lies in the rules of grammar. We refer to the learning of the latter type of information as *structural learning*, and note that it underlies diverse cognitive functions. As humans are exposed to complex rule-governed stimuli — such as music with harmonically related chords or language constrained by the principles of grammar — they acquire knowledge about the material structure without being able to formulate any explicit rules.<sup>1-5</sup> When multiple structures are learned, humans appear to seamlessly switch between performing tasks based on one structure and performing tasks based on another structure, either spontaneously<sup>6</sup> or when driven by an external stimulus.<sup>7</sup> The human ability to learn structure in time-varying stimuli also extends to a marked capacity to fill in missing signals in acoustic or visual inputs,<sup>8,9</sup> and to resolve distinct structures underlying mixed inputs.<sup>10-13</sup> While thus of great relevance for human cognition, the exact mechanisms for structural learning remain unclear.

Over the past two decades, several computational models of neuronal systems have been proposed based on recurrent neural networks (RNNs).<sup>14-23</sup> Notably, these models can successfully learn to generate desired signals with complex dynamical patterns, such as orbits of a damped oscillator,<sup>17</sup> movements of a two-link arm,<sup>16</sup> trajectories from chaotic dynamics,<sup>19-23</sup> and even recurrent spiking dynamics consistent with empirical observations in neural systems.<sup>14,15</sup> Collec-

tively, these prior studies suggest that such models reflect promising candidate mechanisms for learning in the human brain. Here we seek to identify the requisite mechanisms for structural learning, specifically, by building and testing a dynamical systems theory in which the brain is exposed to rule-governed signals generated by chaotic dynamical systems. By developing new theory and performing computational simulations, we demonstrate how and why structural learning and its associated cognitive functions naturally emerge from a unified dynamical systems framework.

### **Dynamical Systems and a General Structural Learning Framework**

A dynamical system consists of a state space and a dynamical rule that determines how the state variable – an instantaneous description of the system – evolves in the state space as a function of time. A trajectory of the dynamical system is a path along which the state variable travels in the state space as time evolves. An attractor is a subset of the state space towards which trajectories tend to evolve. Unlike trajectories on fixed points or periodic orbits, trajectories on a chaotic attractor are sensitive to arbitrarily small differences or changes in initial conditions, yet remain on the attractor throughout all future time points. As a result, a chaotic attractor contains infinite distinct trajectories, all obeying the same dynamical rule. Intuitively, different trajectories on a chaotic attractor can be informally likened to different pieces of music that all follow the same rules of composition, or to different spoken narrations or written passages that all follow the same rules of grammar. Importantly, this relation to dynamical systems is not simply analogical; extensive prior work provides evidence that chaotic attractors are useful generative models for both music and language.<sup>24-29</sup>

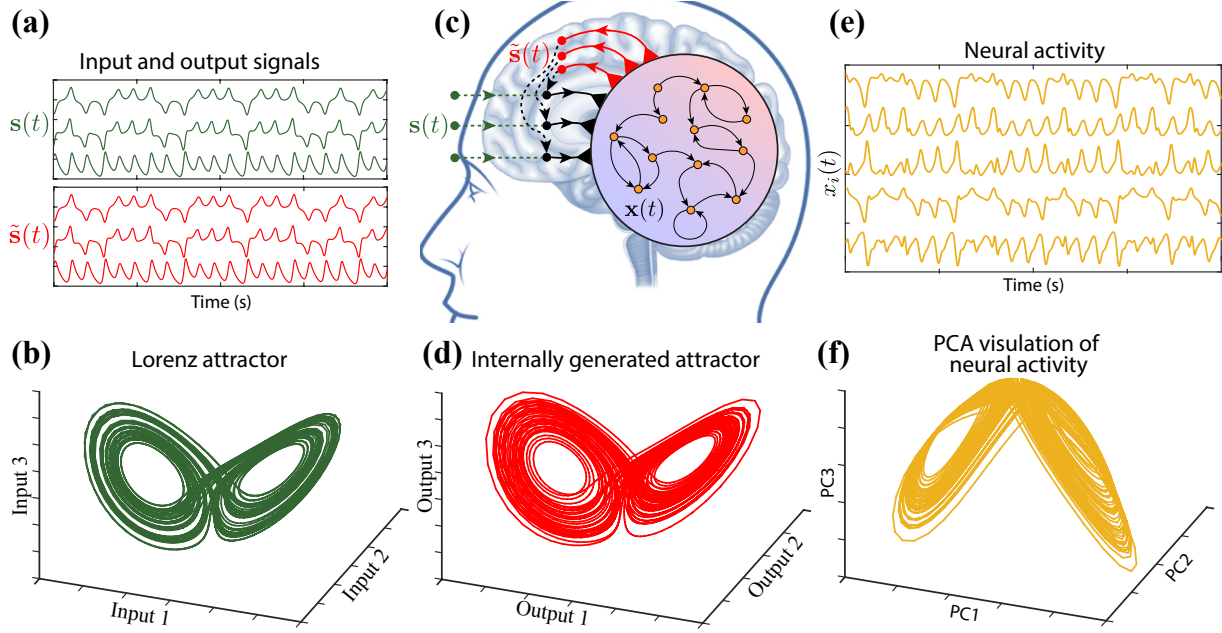


Figure 1: **Dynamical systems framework for structural learning.** (a) A 3-dimensional trajectory  $s(t)$  generated by a Lorenz system as the sensory input (in green), and  $\tilde{s}(t)$  the concurrent output produced by the central system (in red), during the learning phase. (b) A 3-dimensional visualization of a long trajectory on the Lorenz attractor  $\mathcal{A}$ . (c) The general structural learning framework consists of a central system  $x(t)$  and an internally generated output  $\tilde{s}(t)$ . (d) An output trajectory  $\tilde{s}(t)$  that is independently generated during the testing phase, and which follows the learned dynamical rule on the Lorenz attractor. (e) The activity time series of 5 randomly chosen neurons in the central system during the learning phase; the input is shown in panel (a). (f) The first 3 principal components of the  $N$ -dimensional central system activity  $x(t)$  during the learning phase.

Here we use this analytical framework to define the sensory input to the brain as a set of trajectories,  $\mathbf{s}(t) \in \mathbb{R}^n$  in a chaotic attractor  $\mathcal{A} \subset \mathbb{R}^n$ . In other words, the structure of the sensory input is the dynamical rule on the attractor  $\mathcal{A}$ . For concreteness, we choose an  $n = 3$ -dimensional trajectory from a Lorenz attractor<sup>30</sup> (Fig. 1(a,b)). This sensory input is received by the brain, which in turn is modeled as a sophisticated high dimensional dynamical system governed by biophysical laws. We seek to understand how the brain can deduce the underlying dynamical rules of attractors from exemplary trajectories. Furthermore, we seek to understand how the brain can then utilize the acquired dynamical rule to independently generate new trajectories (Fig. 1(c)).

### **Informing the Structural Learning Framework with Underlying Biology**

We seek to build a model that encapsulates three distinct phenomenological features of human structural learning. First, we consider the reinstatement hypothesis, which posits that the content-specific cortical activity at encoding is reinstated as the encoded information is being retrieved.<sup>31,32</sup> Recent evidence supports this idea and suggests that different types of sensory information are encoded in different cortical regions that are reactivated during information retrieval.<sup>33-44</sup> In our model, we therefore recruit a central dynamical system to play the role of the brain regions where sensory information is encoded and stored, and we define its state as  $\mathbf{x}(t) \in \mathbb{R}^N$  (Fig. 1(b)). We operationalize the encoding period as a learning phase, and we operationalize the retrieval period as a testing phase. The central system encodes information during the learning phase as it receives sensory input  $\mathbf{s}(t)$  and evolves following

$$\mathbf{x}(t + 1) = \mathbf{f}(\mathbf{x}(t), \mathbf{s}(t)), \quad (1)$$

where the future state is a function of both the current state  $\mathbf{x}(t)$  and the sensory input  $\mathbf{s}(t)$ .

Second, we consider the presence of an internally generated output, a process thought to enhance and consolidate learned information by interacting with working memory<sup>45,46</sup> (colloquially, this is sometimes called an *inner voice*<sup>45-50</sup>). We model this internally generated output

$$\tilde{\mathbf{s}}(t) = \phi(\mathbf{x}(t)) \quad (2)$$

as being determined by the concurrent state  $\mathbf{x}(t)$  of the central system where  $\phi : \mathbb{R}^N \rightarrow \mathbb{R}^n$ . We let the output function  $\phi(\cdot)$  adapt during the learning phase such that the output  $\tilde{\mathbf{s}}(t)$  can imitate the concurrent input  $\mathbf{s}(t)$  (as shown in Fig. 1(a)). This formulation also becomes useful later as it allows the output  $\tilde{\mathbf{s}}(t)$  to support the dynamics of the central system during the testing phase by omitting the external input  $\mathbf{s}(t)$ .

Third, we consider the recruitment of other cortical regions that support the reinstatement of information during the retrieval process when the external sensory inputs are absent. Beyond the cortical regions that are reactivated as a human mentally rehearses and retrieves sensory information in the absence of exogenous input, other cortical regions also become activated when retrieval begins.<sup>33,51-54</sup> Thus, distinct from the dynamics stipulated by Eq. 1, we model the testing phase dynamics of the central system by the autonomous equation

$$\mathbf{x}(t+1) = \mathbf{f}(\mathbf{x}(t), \tilde{\mathbf{s}}(t)) = \mathbf{f}(\mathbf{x}(t), \phi(\mathbf{x}(t))), \quad (3)$$

where the central system is now driven by the output  $\tilde{\mathbf{s}}(t)$ . This formulation can be thought of intuitively as using one set of connections during the learning phase, and a different set of connections during the testing phase (Fig. 1(c)).

## Instantiating the Informed Structural Learning Framework *in Silico*

To exercise this general structural learning framework, we let the central system be an  $N = 2000$ -node recurrent neural network akin to a reservoir computer:<sup>22,55,56</sup> that is,

$$\mathbf{f}(\mathbf{x}, \mathbf{s}) = \tanh(\mathbf{A}\mathbf{x} + \mathbf{W}_{\text{in}}\mathbf{s} + \mathbf{c}), \quad (4)$$

with  $\mathbf{A} \in \mathbb{R}^{N \times N}$  an adjacency matrix,  $\mathbf{W}_{\text{in}} \in \mathbb{R}^{N \times n}$  an input coefficient matrix, and  $\mathbf{c} \in \mathbb{R}^{N \times 1}$  a constant vector. We also adopt a linear output scheme  $\tilde{\mathbf{s}}(t) = \phi(\mathbf{x}(t)) = \mathbf{W}_{\text{out}}\mathbf{x}(t)$  where the output coefficient matrix  $\mathbf{W}_{\text{out}} \in \mathbb{R}^{n \times N}$  is adaptively updated. Specifically, in the learning phase, we evolve the central system following Eq. 1 where  $\mathbf{s}(t)$  is a trajectory on the Lorenz attractor (Fig. 1(b)), and we adapt the  $\mathbf{W}_{\text{out}}$  in a Hebbian manner according to

$$\mathbf{W}_{\text{out}}(t+1) = \mathbf{W}_{\text{out}}(t) + \alpha \Delta(t) \mathbf{x}^T(t), \quad (5)$$

such that the discrepancy between the input and the output,  $\mathbf{s}(t) - \tilde{\mathbf{s}}(t) = \Delta(t) \in \mathbb{R}^{n \times 1}$ , is reduced.

Intuitively, the output synaptic strength  $[\mathbf{W}_{\text{out}}]_{i,j}$  from neuron  $i$  to the  $j$ -th output  $[\tilde{\mathbf{s}}]_j$ , is modified proportional to the neuronal activity  $[\mathbf{x}]_i$  as well as the discrepancy  $[\Delta]_j$ , where  $\alpha > 0$  is the learning rate. Once  $\mathbf{W}_{\text{out}}$  converges to  $\mathbf{W}_{\text{out}}^*$  where  $|\Delta(t)| \approx 0$ , we remove the external input  $\mathbf{s}$  and evolve the central system following the testing phase dynamics stipulated by Eq. 3. The structural learning is successful if the output  $\tilde{\mathbf{s}}(t) = \mathbf{W}_{\text{out}}^* \mathbf{x}(t)$  that is autonomously generated by the central system follows the same dynamical rule as that of the learned attractor  $\mathcal{A}$ . After instantiating this system *in silico*, we observe that the testing phase output trajectory  $\tilde{\mathbf{s}}(t)$ , although different from the exemplary trajectory in the learning phase, evolves and remains on an attractor similar to the Lorenz attractor (compare Fig. 1(b) and Fig. 1(d)).



## The Structural Learning Function

Here we provide a simple and parsimonious explanation for how structural learning is achieved in our model, akin to a recent study in model-free attractor reconstruction.<sup>57</sup> During the learning phase (Eq. 1), the input trajectory  $\mathbf{s}(t)$  on the chaotic attractor  $\mathcal{A}$  is externally generated by an autonomously evolving input dynamical system, which, together with the central dynamical system, forms a one-way coupled drive-response system. Successful information encoding is guaranteed by the occurrence of an *invertible generalized synchronization* between the input system and the central system:<sup>58–60</sup> the response system  $\mathbf{x}(t)$ , after a transient time from an arbitrary initial condition, becomes uniquely determined by the state of the drive system

$$\mathbf{x}(t) = \psi(\mathbf{s}(t)), \quad (6)$$

where  $\psi : \mathbb{R}^n \rightarrow \mathbb{R}^N$  is a mapping from the drive system to the response system. The image of the attractor  $\mathcal{A}$  under this mapping,  $\psi(\mathcal{A})$ , reflects the central system's internal representation of  $\mathcal{A}$ , denoted by  $\mathcal{P} \subset \mathbb{R}^N$  (Fig. 1(f)).

As  $\mathbf{s}(t)$  evolves on the attractor  $\mathcal{A}$ , the trajectory of the central system  $\mathbf{x}(t)$  in the learning phase evolves toward the manifold  $\mathcal{P}$  (Fig. 1(f)). When  $\psi$  in Eq. 6 is an invertible function on  $\mathcal{A}$ , the encoding of  $\mathcal{A}$  in the internal representation  $\mathcal{P}$  is lossless. The discrepancy  $\Delta = \mathbf{s} - \tilde{\mathbf{s}}$  can be eliminated by adapting the output function  $\phi$  in Eq. 2 towards

$$\phi(\mathbf{x}) = \psi^{-1}(\mathbf{x}), \text{ for } \forall \mathbf{x} \in \mathcal{P}. \quad (7)$$

From the form of this output function, it is clear that the dynamics of the learning phase (Eq. 1) is identical to that of the testing phase (Eq. 3) as long as  $\mathbf{x} \in \mathcal{P}$ . Thus, the output  $\tilde{\mathbf{s}}(t)$  during

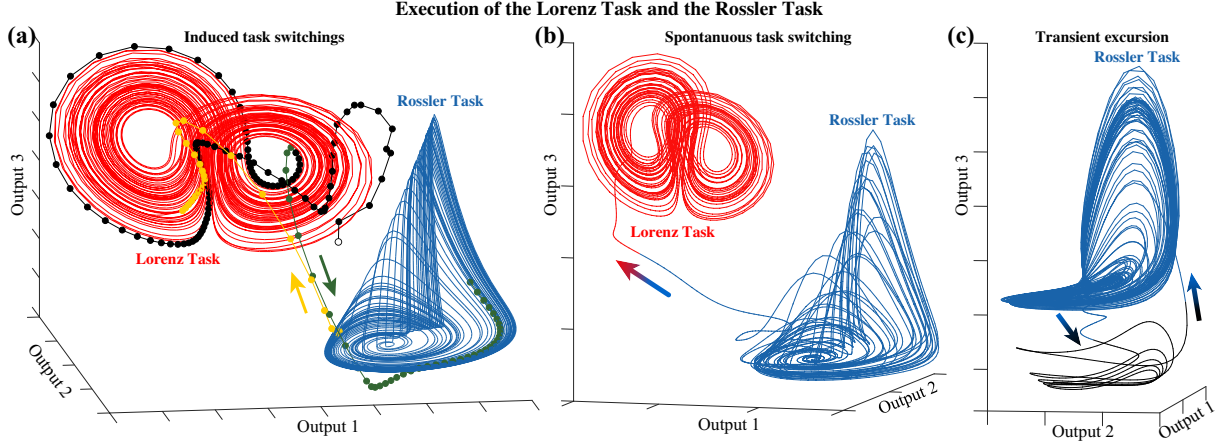


Figure 2: **Learning diverse structures as operationalized by multiple attractors.** (a) We consider two distinct structures from which a stream of stimuli is obtained. We operationalize the two structures as a Lorenz system and a Rössler system. We observe that both structures can be stably learned by a recurrent neural network (RNN). We refer to the learning of each system as a task, and we find that task switchings can be triggered by external cues. (b) Spontaneous task switching from a structure that was not stably learned to a structure that was stably learned. (c) A transient excursion observed when the Rössler system was not stably learned.

the testing phase can evolve following the same dynamical rules as the input  $s(t)$ . To ensure that  $\tilde{s}(t)$  remains on the attractor  $\mathcal{A}$ , we require that the manifold  $\mathcal{P}$  is an attractor of the testing phase dynamics (Eq. 3): that is, the dynamics of the central system is stable to perturbations  $\delta\mathbf{x}$  transverse to the manifold  $\mathcal{P}$ , which can be guaranteed by having all transversal Lyapunov exponents be negative (see Supplement).

### Multistability in Task Switching between Multiple Learned Structures

The occurrence of invertible generalized synchronization permits the structural learning of multiple chaotic attractors,  $\mathcal{A}_k \subset \mathbb{R}^n$  for  $k = 1, 2, \dots, K$ . As the central system is driven by the input trajectory  $s_k(t) \in \mathcal{A}_k$  during the learning phase, the generalized synchronization guarantees that

the central system state  $\mathbf{x}(t)$  evolves correspondingly onto an internal representation manifold

$$\mathcal{P}_k = \psi_k(\mathcal{A}_k), \quad (8)$$

where  $\psi_k : \mathbb{R}^n \rightarrow \mathbb{R}^N$ . If  $\mathcal{P}_k \cap \mathcal{P}_l = \emptyset$  and  $\mathcal{A}_k \cap \mathcal{A}_l = \emptyset$  for  $k \neq l$ , we can neglect the subscript of  $\psi_k$  in Eq. 8. The ideal output function in Eq. 2 for this multitask learning is the one that maps each  $\mathcal{P}_k$  back onto  $\mathcal{A}_k$ , i.e.,  $\mathcal{A}_k = \phi(\mathcal{P}_k)$  for  $k = 1, 2, \dots, K$ . In addition to this ideal output function, if each representation manifold  $\mathcal{P}_k$  is an attractor for the testing phase dynamics (Eq. 3), then the central system learns these tasks such that output trajectories  $\tilde{\mathbf{s}}(t)$  on  $\mathcal{A}_k$  can be stably generated. After instantiating this system *in silico*, we observe that the recurrent neural network from Fig. 1(c) can successfully generate output trajectories  $\tilde{\mathbf{s}}(t)$  that are on the Lorenz attractor and on the Rössler attractor (Fig. 2(a)).

Once multiple attractors  $\mathcal{A}_k$  are learned, it is of interest to consider the phenomenon of task switching by generating  $\tilde{\mathbf{s}}(t)$  from different attractors. When each attractor  $\mathcal{A}_k$  is stably learned, each representation manifold  $\mathcal{P}_k$  becomes an attractor in the dynamics of the testing phase (Eq. 3). Thus, the output trajectory  $\tilde{\mathbf{s}}(t)$  cannot spontaneously depart from one attractor to another. In this case, we can consider explicitly triggering a switch from one task to another (i.e., from one attractor to another attractor). Notice that the generalized synchronization guarantees that, in the testing phase, the central system state  $\mathbf{x}(t)$  converges to  $\psi(\mathbf{s}(t))$  after a short period of time. Thus, we can use a short external input cue,  $\mathbf{s}(t) \in \mathcal{A}_k$ , and lead the central system  $\mathbf{x}$  from an arbitrary state to the desired target manifold  $\mathcal{P}_k$ .

Instantiating these ideas *in silico*, we can begin the testing phase dynamics from a random

initial state  $\mathbf{x}(t = 0)$ . In Fig. 2(a), the output  $\tilde{s}(t)$  evolves following the black dotted line and converges onto the Lorenz attractor  $\mathcal{A}_{\text{Lorenz}}$ . Then, for a very short period of time, we provide an external input  $s(t)$  from a Rössler system. We observed that this external input successfully induced a switch from  $\mathcal{A}_{\text{Lorenz}}$  to  $\mathcal{A}_{\text{Rössler}}$ , as shown by the green dotted line. Thereafter the central system evolves autonomously without any external input for a long period of time, generating the  $\tilde{s}(t)$  of the Rössler attractor. We then use a short Lorenz input  $s(t)$  to drive the central system away from the Rössler attractor and towards the Lorenz attractor, as shown by the yellow dotted line. Thereafter, the central system evolves autonomously with the testing phase dynamics and generates a very long output trajectory on the Lorenz attractor (red).

Next, it is interesting to consider the case in which a few attractors are stably learned while others are not. In this scenario, we would expect spontaneous task switching, independent of any external input. In Fig. 2(b), we consider a case in which the Lorenz system is stably learned but the Rössler system is not. Here we show that starting from an initial condition  $\mathbf{x} \in \mathcal{P}_{\text{Rössler}}$ , the output of the testing phase  $\tilde{s}$  remains on the Rössler attractor (blue) for an extended period of time and then spontaneously departs from the Rössler attractor and converges onto the Lorenz attractor (red). Relatedly, it is interesting to consider the scenario in which a Rössler attractor is only partially learned. In Fig. 2(c), we observe that the output of the testing phase  $\tilde{s}(t)$  exhibits a transient excursion as it evolves on the unstably learned Rössler attractor, in contrast to the dynamics observed in spontaneous task switching.

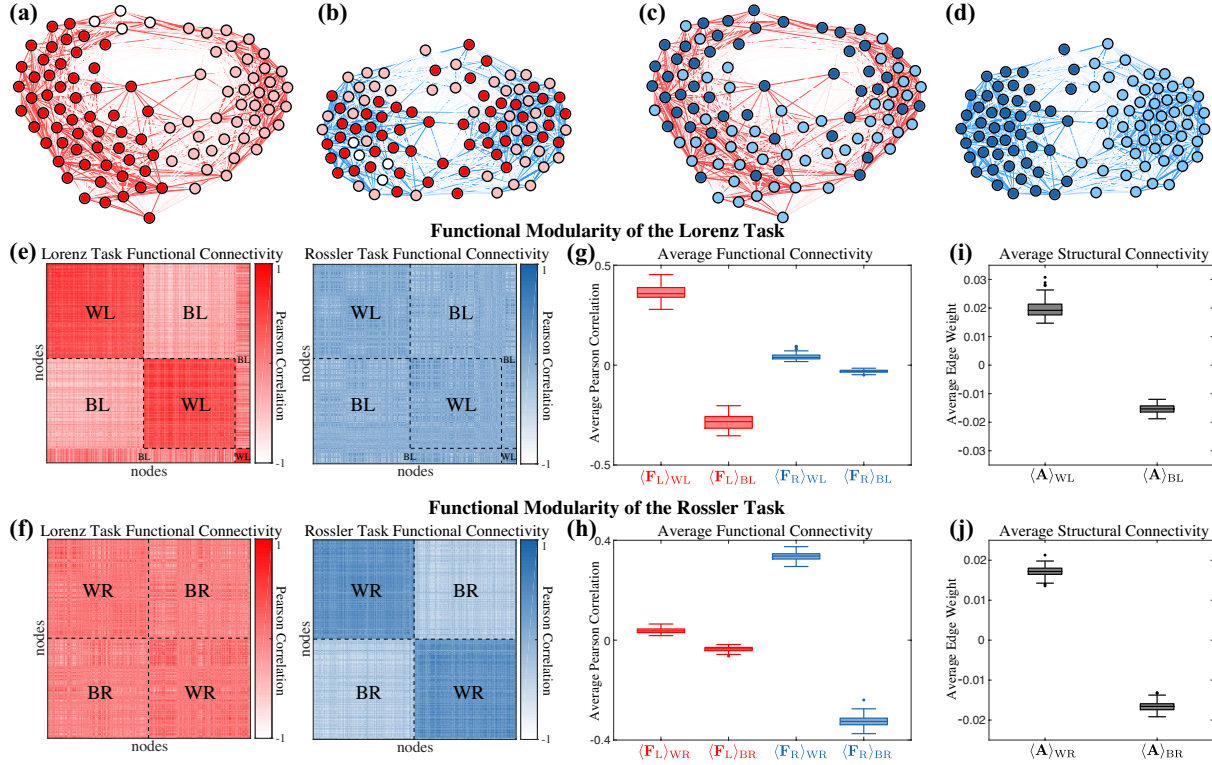


Figure 3: **Task-dependent functional connectome estimated from the statistical similarity in activity time series between neurons.** We show the Lorenz-task (*a,c*) and the Rössler-task (*b,d*) functional connectome for an example RNN using the Force Atlas Layout in Gephi. For the sake of visualization, we only show 100 randomly chosen neurons out of  $N = 2000$ . In panels (*e-f*) we show the full functional connectivity matrices where neurons in panel (*e*) (*f*) are sorted into clusters detected from the Lorenz-task (Rössler-task) functional connectivity matrix using a data-driven community detection algorithm. Neurons in panels (*a,b*) (*c,d*) are colored according to the three (two) clusters detected from the Lorenz-task (Rössler-task) functional connectome. (*g-h*) The average functional connectivity within and between communities as estimated in an ensemble of 100 RNNs. (*i-j*) The average structural connectivity (synaptic weights) within and between communities as estimated in the same ensemble of 100 RNNs.

## Network Mechanics Underlying Multiple Learned Structures

Critically, because the learning of multiple structures is governed by a single equation (Eq. 3), different tasks are executed simply by letting the central system state  $\mathbf{x}(t)$  evolve onto different attractors  $\mathcal{P}_k$ . An important corollary of this fact is that no synapses between units in the RNN are altered, either in their location or in their weight. We will refer to these synapses as structural connections, and note that they are encoded in  $\mathbf{A}$ . While we cannot explain the learning of multiple structures with the pattern of structural connections, it is possible that there is explanatory content in the emergent pattern of functional connections, which are defined as statistical similarities in neuronal time series.

To investigate this possibility, we consider the structural connectivity encoded in the random adjacency matrix  $\mathbf{A} \in \mathbb{R}^{N \times N}$ , and the functional connectivity encoded in the Pearson correlation matrix of the recorded activity  $\mathbf{x}(t) \in \mathbb{R}^{N \times 1}$  for  $t$  during the Lorenz (Rössler) task,  $\mathbf{F}_L \in \mathbb{R}^{N \times N}$  ( $\mathbf{F}_R \in \mathbb{R}^{N \times N}$ ). To summarize the emergent patterns of functional connectivity, we apply a commonly used community detection technique known as modularity maximization to identify groups of neurons that show similar time series. We found strong but distinct community structure in  $\mathbf{F}_L$  and  $\mathbf{F}_R$ . In Fig. 3(e), we show  $\mathbf{F}_L$  (red) and  $\mathbf{F}_R$  (blue) with all nodes sorted by the community structure identified in  $\mathbf{F}_L$ , and in Fig. 3(f), we show  $\mathbf{F}_L$  (red) and  $\mathbf{F}_R$  (blue) with nodes sorted by the community structure identified in  $\mathbf{F}_R$ . These observations indicate that while neurons remain identically structurally connected in both tasks, their emergent collective dynamics differ.

To quantify these observations more fully, we constructed 100 randomly organized and

trained neural networks, and for each we calculated the average functional connectivity among pairs of neurons that are within *versus* between communities identified from either  $\mathbf{F}_L$  or  $\mathbf{F}_R$  (labeled “WL”, “BL”, “WR”, and “BR”, respectively, in Fig. 3(e,f)). In Figs. 3(g,h), we observe that the functional connectivity estimated from the Lorenz task and averaged *within* the communities identified from the Lorenz task data,  $\langle \mathbf{F}_L \rangle_{WL}$ , is significantly larger than the functional connectivity estimated from the Lorenz task and averaged *between* the communities identified from the Lorenz task data,  $\langle \mathbf{F}_L \rangle_{BL}$ . Similarly, for the Rössler task,  $\langle \mathbf{F}_R \rangle_{WR}$  is significantly larger than  $\langle \mathbf{F}_R \rangle_{BR}$ . In contrast, the fact that  $\langle \mathbf{F}_L \rangle_{WR}$  is not significantly larger than  $\langle \mathbf{F}_L \rangle_{WL}$  and similarly  $\langle \mathbf{F}_R \rangle_{WL}$  is not significantly larger than  $\langle \mathbf{F}_R \rangle_{BL}$ , supports our qualitative observation that the community structure in the functional connectivity matrix of the Lorenz task is distinct from the community structure in the functional connectivity matrix of the Rössler task.

Lastly, we asked whether there existed any structural basis for the observed emergent functional communities. Critically, random networks are far from homogeneous, and can display locally dense areas as well as locally sparse areas that occur simply by chance. It is therefore intuitively possible that the random network  $\mathbf{A}$  contains degenerate weak community structure that supports the distinct patterns of emergent dynamics. To investigate this possibility, we calculated the average structural connectivity within the Lorenz communities,  $\langle \mathbf{A} \rangle_{WL}$ , within the Rossler communities,  $\langle \mathbf{A} \rangle_{WR}$ , between the Lorenz communities,  $\langle \mathbf{A} \rangle_{BL}$ , and between the Rossler communities,  $\langle \mathbf{A} \rangle_{BR}$ . We observed greater average structural connectivity within communities than between communities: that is,  $\langle \mathbf{A} \rangle_{WL}$  and  $\langle \mathbf{A} \rangle_{WR}$  were significantly larger than  $\langle \mathbf{A} \rangle_{BL}$  and  $\langle \mathbf{A} \rangle_{BR}$  (Fig. 3(g,h)). This observation motivates two open questions: (i) whether some structural networks

more easily (or less easily) support diverse functional community structures, and thus the learning of multiple systems, and (ii) for a given structural network, can one predict the number of possible emergent community structures, and therefore the number of systems that can be learned.

### **Inferring Missing Variables with the Learned Structure**

Next we consider the problem of inferring missing variables using the learned structure. Given a central system that successfully learns structures of different chaotic attractors  $\mathcal{A}_k$  from input trajectories, we consider the case in which a new trajectory  $s(t)$  on attractor  $\mathcal{A}_k$  is given but with some of the variables  $[s]_i$  missing. The goal is to use the learned structure of  $\mathcal{A}_k$ , together with the remaining variables  $[s]_j$ , to infer values of the missing variables  $[s]_i$ , where  $i \neq j$ . To perform this inference, we evolve the central system following the testing phase dynamics shown in Eq. 1, and we replace the missing variables  $[s]_i$  in  $s$  by the corresponding output variables  $[\tilde{s}]_i$  obtained from Eq. 2 (Fig. 4(a–c)). If the central system driven by available variables  $[s]_j$  maintains the generalized synchronization with the dynamical system that generated the input trajectory, then the inference is expected to be successful.

To instantiate this problem *in silico*, we train an RNN with  $N = 2000$  neurons to learn the structures of both the Lorenz and the Rössler systems. Then, we test the inference of this RNN in three scenarios, where zero, one, and two variables  $[s]_i$  from  $s(t)$  are missing, as schematically depicted in Fig. 4(a–c). The inferred trajectories are the central system output  $\tilde{s}$  during for the Lorenz and the Rössler tasks, respectively. In agreement with intuition, more missing variables



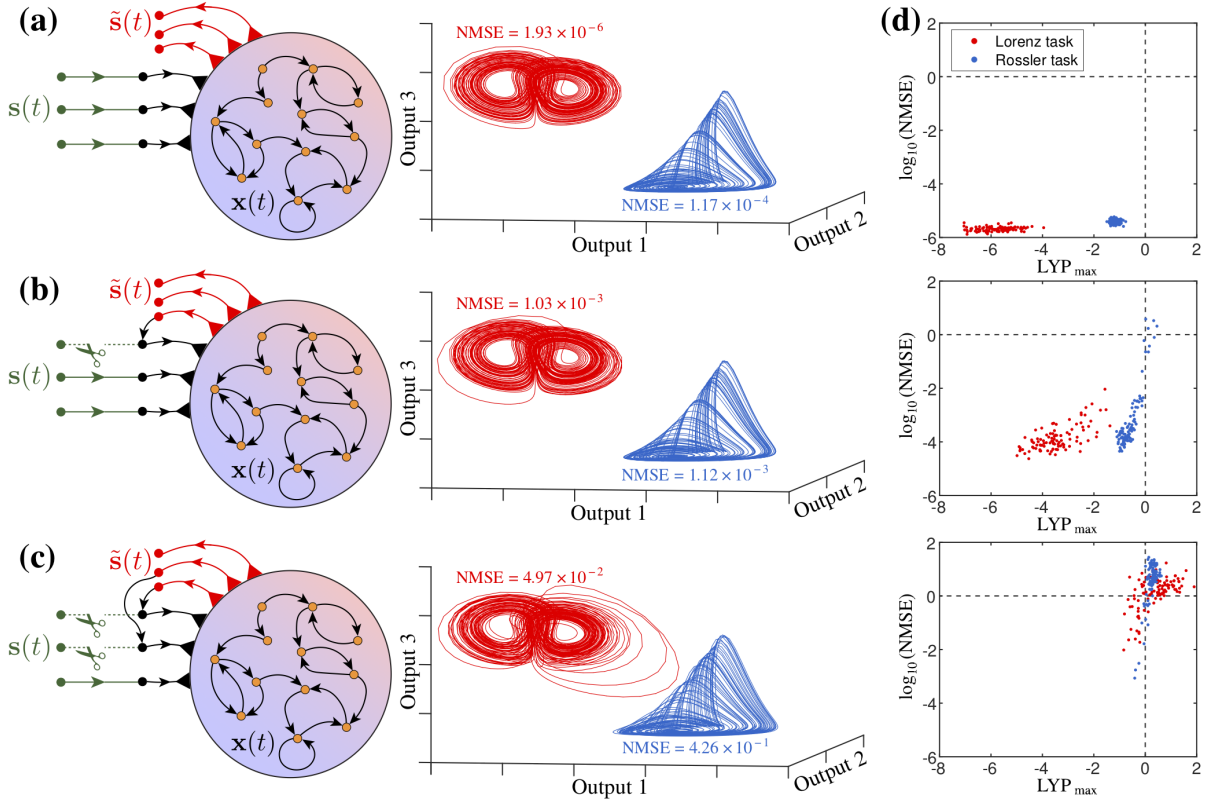


Figure 4: **Inferring the task for both the Lorenz and Rössler systems when full or partial input variables are provided.** (a) The inferred output  $\tilde{s}$  from the central system as well as the normalized mean squared error for the Lorenz (red) and the Rössler (blue) tasks when 3 out of 3 input variables are provided. (b) The inferred output  $\tilde{s}$  from the central system as well as the normalized mean squared error for the Lorenz (red) and the Rössler (blue) tasks when 2 out of 3 input variables are provided. (c) The inferred output  $\tilde{s}$  from the central system as well as the normalized mean squared error for the Lorenz (red) and the Rössler (blue) tasks when 1 out of 3 input variables are provided. (d) The log of the normalized mean squared error in the inferring task with respect to the largest conditional Lyapunov exponents, from 100 randomly constructed neural networks.

leads to poorer inference quality, where the quality is quantified by the normalized mean squared error  $\text{NMSE} = \text{mean}(\|\tilde{\mathbf{s}}(t) - \mathbf{s}(t)\|^2) / \text{var}(\|\mathbf{s}(t)\|^2)$ . To show that the inference quality is related to the quality of the generalized synchronization, we train an ensemble of 100 RNNs and we calculate both their inference error as well as the largest Lyapunov exponent  $\text{LYP}_{\text{max}}$ . A more negative  $\text{LYP}_{\text{max}}$  suggests a stronger generalized synchronization. In Fig. 4(d), we observe that, for the three scenarios, the inference error  $\log_{10}(\text{NMSE})$  is indeed higher whenever the generalized synchronization is weaker; that is, the largest conditional Lyapunov exponent of the central system  $\text{LYP}_{\text{max}}$  is less negative.

### **Deciphering Superimposed Input from Different Dynamical System Sources**

Thus far, we have considered cases in which the external input is a trajectory generated by a single chaotic system. However, the human brain often processes mixed sensory input: a superposition of multiple input trajectories with different structures from distinct sources. Here we show that the mechanism of information encoding in this structural learning framework allows the system to decipher and separate trajectories on different chaotic attractors when the input is their superposition (Fig. 5(a)). Specifically, we consider the 3-dimensional sensory input  $\mathbf{s}_{\text{mix}}(t) = \mathbf{s}_{\text{lor}}(t) + \mathbf{s}_{\text{ros}}(t)$  where  $\mathbf{s}_{\text{lor}}(t)$  and  $\mathbf{s}_{\text{ros}}(t)$  are trajectories on the Lorenz attractor  $\mathcal{A}_{\text{Lorenz}}$  and on the Rössler attractor  $\mathcal{A}_{\text{Rössler}}$ , respectively. Again the central system is modeled as an RNN (Eq. (4)) and is evolved following the learning phase dynamics (Eq. 1) with the external input  $\mathbf{s} = \mathbf{s}_{\text{mix}}$ . In this case, two 3-dimensional outputs  $\tilde{\mathbf{s}}_{\text{lor}}(t) = \mathbf{W}_{\text{lor}}\mathbf{x}(t)$  and  $\tilde{\mathbf{s}}_{\text{ros}}(t) = \mathbf{W}_{\text{ros}}\mathbf{x}(t)$  are learned to match with the actual Lorenz trajectory  $\mathbf{s}_{\text{lor}}(t)$  and the actual Rössler trajectory  $\mathbf{s}_{\text{ros}}(t)$ . This is done by adapting

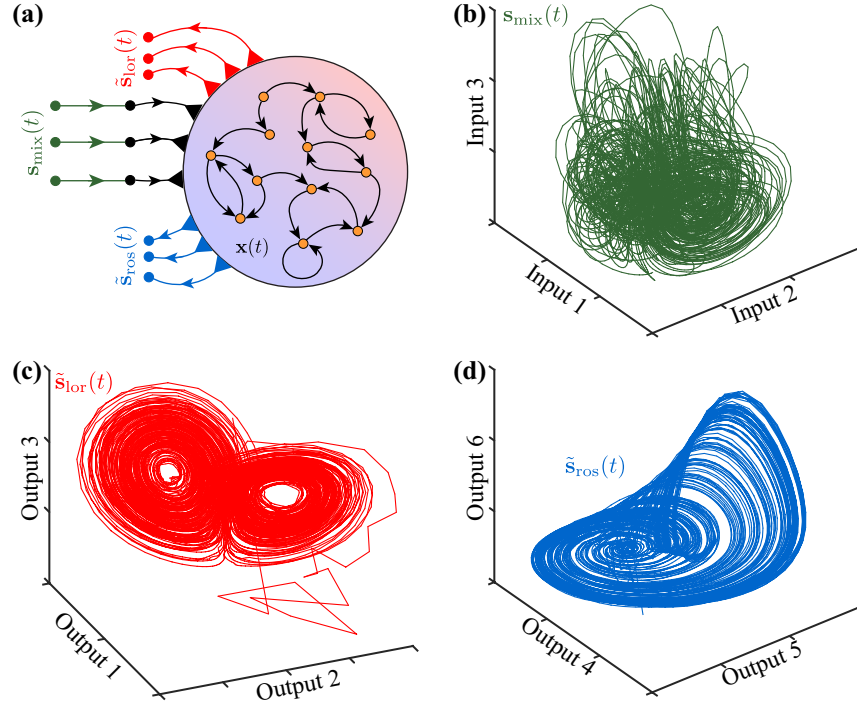


Figure 5: **Structural learning framework used to decipher mixed input signal from the Lorenz and the Rössler systems.** (a) The structural learning framework for deciphering superimposed input. The central system is driven by 3-dimensional superimposed input  $s_{\text{mix}}(t) = s_{\text{lor}}(t) + s_{\text{ros}}(t)$ . During the learning phase, the output weight matrices for the two 3-dimensional outputs  $\tilde{s}_{\text{lor}}$  and  $\tilde{s}_{\text{ros}}$  approximate the concurrent Lorenz trajectory  $s_{\text{lor}}$  and Rössler trajectory  $s_{\text{ros}}(t)$ . (b) The testing phase input trajectory to the central system,  $s_{\text{mix}}$ , which is a superposition of a new Lorenz trajectory and a new Rössler trajectory, both different from the exemplary trajectories used in learning phase. (c) The deciphered  $\tilde{s}_{\text{lor}}$  by this model during the testing phase. After a transient excursion from the initial state, the deciphered output converges to a good approximation of the actual Lorenz trajectory. (d) The deciphered  $\tilde{s}_{\text{ros}}$  by this model during the testing phase. After a transient excursion from the initial state, the deciphered output converges to a good approximation of the actual Rössler trajectory.

the weight matrices  $\mathbf{W}_{\text{lor}}$  and  $\mathbf{W}_{\text{ros}}$  following Eq. (5) where the errors  $\Delta(t)$  are correspondingly  $\mathbf{s}_{\text{lor}}(t) - \tilde{\mathbf{s}}_{\text{lor}}(t)$  and  $\mathbf{s}_{\text{ros}}(t) - \tilde{\mathbf{s}}_{\text{ros}}(t)$ . After the learning phase, we start the system from a random initial state  $\mathbf{x}(t = 0)$  and evolve the central system following Eq. (1) with a mixed input  $\mathbf{s}_{\text{mix}}$  that is distinct from the exemplary trajectory used in the learning phase (Fig. 5(b)). In Fig. 5(c,d), we observe that the central system successfully separates the mixed trajectory into outputs  $\tilde{\mathbf{s}}_{\text{lor}}(t)$  and  $\tilde{\mathbf{s}}_{\text{ros}}(t)$  which are good estimations of the actual Lorenz trajectory  $\mathbf{s}_{\text{lor}}(t)$  and the actual Rössler trajectory  $\mathbf{s}_{\text{ros}}(t)$ .

As observed empirically,<sup>10</sup> although the input is mixed, the streams of stimuli from distinct underlying structures are encoded separately, thereby supporting selective listening. To demonstrate this same phenomenon in our theoretical framework, we consider the direct product of the Lorenz system and the Rössler system as a combined dynamical system. The state variable of this combined system is  $\mathbf{s}_{\text{cob}}(t) = [\mathbf{s}_{\text{lor}}(t), \mathbf{s}_{\text{ros}}(t)] \in \mathbb{R}^6$ . As  $\mathbf{s}_{\text{lor}}$  and  $\mathbf{s}_{\text{ros}}$  evolve onto the Lorenz attractor  $\mathcal{A}_{\text{Lorenz}}$  and the Rössler attractor  $\mathcal{A}_{\text{Rössler}}$ , respectively, the combined system state  $\mathbf{s}_{\text{cob}}$  evolves onto an attractor that is the Cartesian product of the two attractors,  $\mathcal{A}_{\text{cob}} = \mathcal{A}_{\text{Lorenz}} \times \mathcal{A}_{\text{Rössler}} \subset \mathbb{R}^6$ . Since one can do a simple coordinate transformation from  $\mathbf{s}_{\text{cob}} = [\mathbf{s}_{\text{lor}}, \mathbf{s}_{\text{ros}}]$  to  $[\mathbf{s}_{\text{lor}} + \mathbf{s}_{\text{ros}}, \mathbf{s}_{\text{lor}} - \mathbf{s}_{\text{ros}}]$ , we note that the mixed input  $\mathbf{s}_{\text{mix}} = \mathbf{s}_{\text{lor}} + \mathbf{s}_{\text{ros}}$  is essentially a 3-dimensional projection of the 6-dimensional  $\mathbf{s}_{\text{cob}}$ . Although the central system is one-way coupled to the combined dynamics through the mixed input  $\mathbf{s}_{\text{mix}}$  rather than the full state variable  $\mathbf{s}_{\text{cob}}$ , the generalized synchronization<sup>58–60</sup> can guarantee that the central system state  $\mathbf{x}$  converges to  $\psi(\mathbf{s}_{\text{cob}})$  for  $\mathbf{s}_{\text{cob}} \in \mathcal{A}_{\text{cob}}$ . If the generalized synchronization function  $\psi$  is invertible, the internal representation  $\psi(\mathbf{s}_{\text{cob}})$  separately encodes the information in  $\mathbf{s}_{\text{lor}}$  and  $\mathbf{s}_{\text{ros}}$ , rather than the superimposed  $\mathbf{s}_{\text{lor}} + \mathbf{s}_{\text{ros}}$ . Thus, either the

information of the Lorenz or the Rössler attractors can be retrieved when the system adapts the output weight matrices towards  $\mathbf{W}_{\text{lor}}^*$  and  $\mathbf{W}_{\text{ros}}^*$  that approximate the inverse function  $\psi^{-1}(\cdot)$ , i.e.,  $[\mathbf{W}_{\text{lor}}^*, \mathbf{W}_{\text{ros}}^*]\mathbf{x} \approx \psi^{-1}(\mathbf{x})$ .

## Conclusion

Humans appear to effortlessly learn abstract structures from raw time-evolving material and then use those structures to compose new data, to infer missing data, or even to decipher mixed data. Many computational models have been proposed under a Bayesian-brain hypothesis that shed light on how humans might learn hidden properties from a few relevant experiences.<sup>61–68</sup> Complementing these probabilistic models, we propose a general dynamical system based model derived from first principles. Surprisingly, this simple dynamical model produces successful learning of underlying structures (i.e., dynamical properties of chaotic attractors) from raw materials (i.e., exemplary trajectories on these attractors). We show that this dynamical system can create new streams of data with the learned structure, infer missing data, and both learn and operate different tasks by visiting different attractors in the system’s representational space. With its generality, we believe that this framework serves as a promising preliminary model to which more biological details could be added in future to prompt better performance, such as rules of adaption that may lead to better encoding as well as larger learning capacity.

1. Bly, B. M., Carrión, R. E. & Rasch, B. Domain-specific learning of grammatical structure in musical and phonological sequences. *Memory & cognition* **37**, 10–20 (2009).
2. Tillmann, B., Bharucha, J. J. & Bigand, E. Implicit learning of tonality: a self-organizing approach. *Psychological review* **107**, 885 (2000).
3. Aldwell, E. & Schachter, C. Harmony & voice leading, schirmer, 2003. *ISBN: 0-15-506242-5*.
4. Kostka, S. M., Payne, D. & Almén, B. Tonal harmony, with an introduction to twentieth-century music. 4th (2000).
5. Besson, M. & Schön, D. Comparison between language and music. *Annals of the New York Academy of Sciences* **930**, 232–258 (2001).
6. Kessler, Y., Shencar, Y. & Meiran, N. Choosing to switch: Spontaneous task switching despite associated behavioral costs. *Acta Psychologica* **131**, 120–128 (2009).
7. Koch, I. & Allport, A. Cue-based preparation and stimulus-based priming of tasks in task switching. *Memory & cognition* **34**, 433–444 (2006).
8. Constantino, F. C. & Simon, J. Z. Dynamic cortical representations of perceptual filling-in for missing acoustic rhythm. *Scientific reports* **7**, 17536 (2017).
9. Komatsu, H. The neural mechanisms of perceptual filling-in. *Nature reviews neuroscience* **7**, 220 (2006).

10. Ding, N. & Simon, J. Z. Emergence of neural encoding of auditory objects while listening to competing speakers. *Proceedings of the National Academy of Sciences* **109**, 11854–11859 (2012).
11. Xiang, J., Simon, J. & Elhilali, M. Competing streams at the cocktail party: exploring the mechanisms of attention and temporal integration. *Journal of Neuroscience* **30**, 12084–12093 (2010).
12. Luo, H. & Poeppel, D. Phase patterns of neuronal responses reliably discriminate speech in human auditory cortex. *Neuron* **54**, 1001–1010 (2007).
13. Mesgarani, N. & Chang, E. F. Selective cortical representation of attended speaker in multi-talker speech perception. *Nature* **485**, 233 (2012).
14. Rajan, K., Harvey, C. D. & Tank, D. W. Recurrent network models of sequence generation and memory. *Neuron* **90**, 128–142 (2016).
15. Alemi, A., Machens, C., Denève, S. & Slotine, J.-J. Learning arbitrary dynamics in efficient, balanced spiking networks using local plasticity rules. *arXiv preprint arXiv:1705.08026* (2017).
16. Gilra, A. & Gerstner, W. Predicting non-linear dynamics: a stable local learning scheme for recurrent spiking neural networks. *arXiv preprint arXiv:1702.06463* (2017).
17. Denève, S., Alemi, A. & Bourdoukan, R. The brain as an efficient and robust adaptive learner. *Neuron* **94**, 969–977 (2017).

18. Abbott, L., DePasquale, B. & Memmesheimer, R.-M. Building functional networks of spiking model neurons. *Nature neuroscience* **19**, 350 (2016).
19. Maass, W., Natschläger, T. & Markram, H. Real-time computing without stable states: A new framework for neural computation based on perturbations. *Neural computation* **14**, 2531–2560 (2002).
20. Jaeger, H. & Haas, H. Harnessing nonlinearity: Predicting chaotic systems and saving energy in wireless communication. *science* **304**, 78–80 (2004).
21. Sussillo, D. & Abbott, L. F. Generating coherent patterns of activity from chaotic neural networks. *Neuron* **63**, 544–557 (2009).
22. Pathak, J., Lu, Z., Hunt, B. R., Girvan, M. & Ott, E. Using machine learning to replicate chaotic attractors and calculate lyapunov exponents from data. *Chaos: An Interdisciplinary Journal of Nonlinear Science* **27**, 121102 (2017).
23. Pathak, J., Hunt, B., Girvan, M., Lu, Z. & Ott, E. Model-free prediction of large spatiotemporally chaotic systems from data: A reservoir computing approach. *Physical Review Letters* **120**, 024102 (2018).
24. Mayer-Kress, G., Bargar, R. & Choi, I. *Musical structures in data from chaotic attractors* (University of Illinois at Urbana-Champaign, 1992).
25. Elman, J. L. Language as a dynamical system. *Mind as motion: Explorations in the dynamics of cognition* 195–225 (1995).



26. Winters, R. M. Musical mapping of chaotic attractors. *Wooster, Ohio, EE. UU.: Physics Department, The College of Wooster* (2009).
27. Bidlack, R. Chaotic systems as simple (but complex) compositional algorithms. *Computer Music Journal* **16**, 33–47 (1992). URL <http://www.jstor.org/stable/3680849>.
28. Castilho, P. L. Chaotic systems as compositional algorithms mus-15 (2015).
29. Mackenzie, J. P. Chaotic predictive modelling of sound. In *ICMC* (Citeseer, 1995).
30. Lorenz, E. N. Deterministic nonperiodic flow. *Journal of the atmospheric sciences* **20**, 130–141 (1963).
31. James, W. The principles of psychology (new york: Henry holt and company) (1890).
32. Tulving, E. & Thomson, D. M. Encoding specificity and retrieval processes in episodic memory. *Psychological review* **80**, 352 (1973).
33. Wheeler, M. E., Petersen, S. E. & Buckner, R. L. Memory’s echo: vivid remembering reactivates sensory-specific cortex. *Proceedings of the National Academy of Sciences* **97**, 11125–11129 (2000).
34. Kragel, J. E. *et al.* Similar patterns of neural activity predict memory function during encoding and retrieval. *NeuroImage* **155**, 60–71 (2017).
35. Nyberg, L., Habib, R., McIntosh, A. R. & Tulving, E. Reactivation of encoding-related brain activity during memory retrieval. *Proceedings of the National Academy of Sciences* **97**, 11120–11124 (2000).

36. Düzel, E. *et al.* Human hippocampal and parahippocampal activity during visual associative recognition memory for spatial and nonspatial stimulus configurations. *Journal of Neuroscience* **23**, 9439–9444 (2003).
37. Khader, P., Burke, M., Bien, S., Ranganath, C. & Rösler, F. Content-specific activation during associative long-term memory retrieval. *NeuroImage* **27**, 805–816 (2005).
38. Ranganath, C., Heller, A., Cohen, M. X., Brozinsky, C. J. & Rissman, J. Functional connectivity with the hippocampus during successful memory formation. *Hippocampus* **15**, 997–1005 (2005).
39. Woodruff, C. C., Johnson, J. D., Uncapher, M. R. & Rugg, M. D. Content-specificity of the neural correlates of recollection. *Neuropsychologia* **43**, 1022–1032 (2005).
40. Slotnick, S. D. & Schacter, D. L. The nature of memory related activity in early visual areas. *Neuropsychologia* **44**, 2874–2886 (2006).
41. Johnson, J. D. & Rugg, M. D. Recollection and the reinstatement of encoding-related cortical activity. *Cerebral Cortex* **17**, 2507–2515 (2007).
42. Diana, R. A., Yonelinas, A. P. & Ranganath, C. Parahippocampal cortex activation during context reinstatement predicts item recollection. *Journal of Experimental Psychology: General* **142**, 1287 (2013).
43. Rugg, M. D. & Vilberg, K. L. Brain networks underlying episodic memory retrieval. *Current opinion in neurobiology* **23**, 255–260 (2013).

44. Bosch, S. E., Jehee, J. F., Fernández, G. & Doeller, C. F. Reinstatement of associative memories in early visual cortex is signaled by the hippocampus. *Journal of Neuroscience* **34**, 7493–7500 (2014).
45. Marvel, C. L. & Desmond, J. E. From storage to manipulation: how the neural correlates of verbal working memory reflect varying demands on inner speech. *Brain and language* **120**, 42–51 (2012).
46. Perrone-Bertolotti, M., Rapin, L., Lachaux, J.-P., Baciú, M. & Loevenbruck, H. What is that little voice inside my head? inner speech phenomenology, its role in cognitive performance, and its relation to self-monitoring. *Behavioural brain research* **261**, 220–239 (2014).
47. Baddeley, A., Hitch, G. & Bower, G. Recent advances in learning and motivation. *Working memory* **8**, 647–667 (1974).
48. Morin, A., Uttl, B. & Hamper, B. Self-reported frequency, content, and functions of inner speech. *Procedia-Social and Behavioral Sciences* **30**, 1714–1718 (2011).
49. Williams, D. M., Bowler, D. M. & Jarrold, C. Inner speech is used to mediate short-term memory, but not planning, among intellectually high-functioning adults with autism spectrum disorder. *Development and psychopathology* **24**, 225–239 (2012).
50. Alderson-Day, B. & Fernyhough, C. Inner speech: development, cognitive functions, phenomenology, and neurobiology. *Psychological bulletin* **141**, 931 (2015).

51. Addis, D. R., Wong, A. T. & Schacter, D. L. Remembering the past and imagining the future: common and distinct neural substrates during event construction and elaboration. *Neuropsychologia* **45**, 1363–1377 (2007).
52. Kosslyn, S. M., Ganis, G. & Thompson, W. L. Neural foundations of imagery. *Nature Reviews Neuroscience* **2**, 635 (2001).
53. Halpern, A. R. & Zatorre, R. J. When that tune runs through your head: a pet investigation of auditory imagery for familiar melodies. *Cerebral cortex* **9**, 697–704 (1999).
54. Buckner, R. L. & Carroll, D. C. Self-projection and the brain. *Trends in cognitive sciences* **11**, 49–57 (2007).
55. Lu, Z. *et al.* Reservoir observers: Model-free inference of unmeasured variables in chaotic systems. *Chaos: An Interdisciplinary Journal of Nonlinear Science* **27**, 041102 (2017).
56. Pathak, J., Hunt, B., Girvan, M., Lu, Z. & Ott, E. Model-free prediction of large spatiotemporally chaotic systems from data: A reservoir computing approach. *Phys. Rev. Lett.* **120**, 024102 (2018). URL <https://link.aps.org/doi/10.1103/PhysRevLett.120.024102>.
57. Lu, Z., Hunt, B. R. & Ott, E. Attractor reconstruction by machine learning. *Chaos: An Interdisciplinary Journal of Nonlinear Science* **28**, 061104 (2018). URL <https://doi.org/10.1063/1.5039508>. <https://doi.org/10.1063/1.5039508>.
58. Afraimovich, V., Verichev, N. & Rabinovich, M. I. Stochastic synchronization of oscillation in dissipative systems. *Radiophysics and Quantum Electronics* **29**, 795–803 (1986).

59. Pecora, L. M. & Carroll, T. L. Synchronization in chaotic systems. *Phys. Rev. Lett.* **64**, 821–824 (1990). URL <https://link.aps.org/doi/10.1103/PhysRevLett.64.821>.
60. Rulkov, N. F., Sushchik, M. M., Tsimring, L. S. & Abarbanel, H. D. Generalized synchronization of chaos in directionally coupled chaotic systems. *Physical Review E* **51**, 980 (1995).
61. Lake, B. M., Salakhutdinov, R. & Tenenbaum, J. B. Human-level concept learning through probabilistic program induction. *Science* **350**, 1332–1338 (2015).
62. Battaglia, P. W., Hamrick, J. B. & Tenenbaum, J. B. Simulation as an engine of physical scene understanding. *Proceedings of the National Academy of Sciences* **110**, 18327–18332 (2013).
63. Tenenbaum, J. B., Kemp, C., Griffiths, T. L. & Goodman, N. D. How to grow a mind: Statistics, structure, and abstraction. *science* **331**, 1279–1285 (2011).
64. Chater, N., Oaksford, M., Hahn, U. & Heit, E. Bayesian models of cognition. *Wiley Interdisciplinary Reviews: Cognitive Science* **1**, 811–823 (2010).
65. Griffiths, T. L., Kemp, C. & Tenenbaum, J. B. Bayesian models of cognition (2008).
66. Kemp, C. & Tenenbaum, J. B. The discovery of structural form. *Proceedings of the National Academy of Sciences* **105**, 10687–10692 (2008).
67. Chater, N., Tenenbaum, J. B. & Yuille, A. Probabilistic models of cognition: Conceptual foundations (2006).

68. Tenenbaum, J. B., Griffiths, T. L. & Kemp, C. Theory-based bayesian models of inductive learning and reasoning. *Trends in cognitive sciences* **10**, 309–318 (2006).

**Acknowledgements** We thank Elisabeth A. Karuza, Christopher W. Lynn, Jason Z. Kim, and Arian Ashourvan for helpful comments on earlier versions of this manuscript. ZL and DSB acknowledge support from the John D. and Catherine T. MacArthur Foundation, the Alfred P. Sloan Foundation, the ISI Foundation, the Paul Allen Foundation, the Army Research Laboratory (W911NF-10-2-0022), the Army Research Office (Bassett-W911NF-14-1-0679, Grafton-W911NF-16-1-0474, DCIST-W911NF-17-2-0181), the Office of Naval Research, the National Institute of Mental Health (2-R01-DC-009209-11, R01-MH112847, R01-MH107235, R21-MH-106799), the National Institute of Child Health and Human Development (1R01HD086888-01), National Institute of Neurological Disorders and Stroke (R01 NS099348), and the National Science Foundation (BCS-1441502, BCS-1430087, NSF PHY-1554488 and BCS-1631550). The content is solely the responsibility of the authors and does not necessarily represent the official views of any of the funding agencies.

**Competing Interests** The authors declare that they have no competing financial interests.

**Correspondence** Correspondence and requests for materials should be addressed to dsb@seas.upenn.edu.

# A Parsimonious Dynamical Model for Structural Learning in the Human Brain

## *Supplementary Information*

In this document, we further discuss the general structural learning framework from the perspective of dynamical systems, and we provide technical details regarding the *in silico* instantiations. Specifically, in Sec. 1 we discuss information encoding during the learning phase with an emphasis on invertible generalized synchronization. In Sec. 2, we discuss how transverse stability affects the system's performance during the testing phase. In Secs. 3–5, we provide the technical details of how we implement recurrent neural networks to learn structures of the Lorenz and the Rössler attractors. In Sec. 6 we compare our study to prior work.

### **1 Information Encoding in the Learning Phase**

Successful information encoding is guaranteed by the invertible generalized synchronization between the input system and the central system. During the learning phase, the central system is one-way coupled to the input dynamical system,

$$\mathbf{s}(t + 1) = \mathbf{g}(\mathbf{s}(t)), \quad (9)$$

where  $\mathbf{s} \in \mathbb{R}^n$  and the time is discrete. For inputs that are generated by continuous-time dynamical systems (e.g., the Lorenz system or the Rössler system), Eq. (9) is still a valid description as  $\mathbf{g}(\cdot)$  can be interpreted as an evolution function that maps  $\mathbf{s}$  forward along its trajectory by a time step  $\tau$ . The central system in the learning phase evolves non-autonomously following,

$$\mathbf{x}(t + 1) = \mathbf{f}(\mathbf{x}(t), \mathbf{s}(t)), \quad (10)$$

as it is driven by the input  $s(t)$  generated by Eq. (9). In the main manuscript, we consider cases where  $s(t)$  evolves onto an invariant manifold  $\mathcal{A}$  that is a strange attractor. However, we note that the theory also works for simpler invariant manifolds such as limit cycles and fixed points.

**Generalized synchronization.** Encoding the input into the central system requires that the central system state becomes uniquely determined by the concurrent input system state, i.e.,  $\mathbf{x}(t) = \psi(s(t))$ . Thus, we say that generalized synchronization occurs between the input system and the central system.<sup>58–60</sup> Although we only discuss cases where  $s$  evolves on invariant manifolds  $\mathcal{A}$  that are strange attractors, our approach also applies in cases where  $\mathcal{A}$  is a limit cycle or a stable fixed point.

**The largest conditional Lyapunov exponent.** One common criterion of generalized synchronization is the sign of the largest conditional Lyapunov exponent of the non-autonomous response system.<sup>59</sup> Thus, in our study, we calculate the largest conditional Lyapunov exponent  $\lambda_{\max}$  of the non-autonomous central system (Eq. (10)) as a criterion for the information encoding during the learning phase. To calculate  $\lambda_{\max}$ , we evolve the learning phase central system (Eq. (10)) with a particular input trajectory  $s(t) \in \mathcal{A}$ , from two closeby random initial states,  $\mathbf{x}(0)$  and  $\mathbf{x}'(0) = \mathbf{x}(0) + \boldsymbol{\delta}_0$ , where  $\|\boldsymbol{\delta}_0\|_2 \ll 1$ . The largest conditional Lyapunov exponent  $\lambda_{\max}$  is then the exponential convergence or divergence rate of the distance  $\boldsymbol{\delta}_t = \mathbf{x}'(t) - \mathbf{x}(t)$  between these two trajectories,

$$\lambda_{\max} = \lim_{T \rightarrow \infty} \frac{1}{T} \log\left(\frac{\|\boldsymbol{\delta}_t\|_2}{\|\boldsymbol{\delta}_0\|_2}\right). \quad (11)$$



Notice that the distance  $\delta_t$  evolves following,

$$\delta_{t+1} = \mathbf{J}(t)\delta_t, \quad (12)$$

where  $\mathbf{J}(t) \in \mathbb{R}^{N \times N}$  is the Jacobian matrix of  $\mathbf{f}(\cdot, \cdot)$ ,

$$\mathbf{J}(t) = \left. \frac{\partial \mathbf{f}(\mathbf{x}, \mathbf{s})}{\partial \mathbf{x}} \right|_{\mathbf{x}=\mathbf{x}(t), \mathbf{s}=\mathbf{s}(t)}. \quad (13)$$

With Eqs. (11-13), we estimate the largest Lyapunov exponent  $\lambda_{\max}$ , given a fairly long trajectory  $\mathbf{x}(t)$  and the accompanying input trajectory  $\mathbf{s}(t)$ . If  $\lambda_{\max} < 0$ , we say that the central system is generally synchronized to the input system, and the input information is encoded into the central system in the form of  $\mathbf{x} = \psi(\mathbf{s})$ .

**Lossless encoding.** To guarantee that the information encoded in the central system is lossless, the generalized synchronization mapping function  $\psi : \mathcal{A} \rightarrow \mathcal{P}$  should be one-to-one from  $\mathcal{A}$  to  $\mathcal{P}$ , where  $\mathcal{A} \subset \mathbb{R}^n$  and  $\mathcal{P} \subset \mathbb{R}^N$ . In the main text, we enforce this to be true by wisely designing the central system. In practice, this one-to-one encoding is likely to be achieved when one employs a high dimensional central system with  $N \gg n$ . The tuition behind this choice of large  $N$  is that, based on the weak Whitney embedding theorem, the function  $\psi$  is likely to be one-to-one if the dimension of  $\mathcal{P}$  is greater than twice the dimension of the manifold  $\mathcal{A}$ .

## 2 Transverse Stability and the Testing Phase Performance

When the central system changes from the learning phase architecture to the testing phase architecture, it becomes an autonomous dynamical system,

$$\mathbf{x}(t+1) = \mathbf{f}(\mathbf{x}(t), \phi(\mathbf{x}(t))), \quad (14)$$

as it replaces the external input  $s(t)$  in Eq. (10) with a self-generated output  $\tilde{s}(t) = \phi(\mathbf{x}(t))$ . Ideally, the learning adapts the output function towards  $\phi^*$  such that  $\phi^*(\mathbf{x}) = \psi^{-1}(\mathbf{x})$  for any trajectory  $\mathbf{x} = \psi(s)$  as long as  $s$  is a trajectory on  $\mathcal{A}$  generated by the input system. Thus, the attractor  $\mathcal{A} \subset \mathbb{R}^n$  is said to be embedded into the autonomous central system as an invariant manifold  $\mathcal{P} \subset \mathbb{R}^N$  where  $\mathcal{P} = \psi(\mathcal{A})$  because, for any input trajectory  $s$  on  $\mathcal{A}$ , the trajectory  $\mathbf{x} = \psi(s)$  is a solution of the autonomous central system Eq. (14). In practice however, there always exists noise in the central system as well as a mismatch between  $\phi$  and the ideal  $\phi^*$ . Thus, to make sure the central system evolves stably on  $\mathcal{P}$ , we require that the  $\mathcal{P}$  is not only an invariant manifold but an attractor of Eq. (14). If that is the case, then all of the Lyapunov exponents of the autonomous central system should be negative except for those non-negative exponents that are inherited directly from the chaotic attractor  $\mathcal{A}$ .<sup>57</sup>

### 3 Preparing Input Trajectories from Chaotic Systems

In this paper, we consider two widely studied 3-dimensional chaotic dynamical systems: the Lorenz system and the Rössler system.

**Input trajectory from the Lorenz sytem.** The input trajectory  $s_{\text{lor}}(t)$  from the Lorenz system is generated as follows. We integrate the differential equations of the Lorenz system

$$\begin{aligned}
 \frac{d}{dt}X_{\text{lor}} &= 10Y_{\text{lor}} - 10X_{\text{lor}}, \\
 \frac{d}{dt}Y_{\text{lor}} &= -X_{\text{lor}}Z_{\text{lor}} + 28X_{\text{lor}} - Y_{\text{lor}}, \\
 \frac{d}{dt}Z_{\text{lor}} &= X_{\text{lor}}Y_{\text{lor}} - 8Z_{\text{lor}}/3,
 \end{aligned} \tag{15}$$

using a 4-th order Runge-Kutta integrator with time step  $\delta t = 10^{-3}$  from a random initial state. Each of the three variables  $X_{\text{lor}}$ ,  $Y_{\text{lor}}$ , and  $Z_{\text{lor}}$  of the trajectory is then normalized to have a mean of zero and a variance of one. This renormalized trajectory is then saved as the Lorenz-task input trajectory  $\mathbf{s}_{\text{lor}}(t)$  with time resolution  $\tau = 0.02$ .

**Input trajectory from the Rössler system.** Similar to the Lorenz system, the input trajectory  $\mathbf{s}_{\text{ros}}(t)$  from the Rössler system is generated as follows. We integrate the differential equation of the Rössler system

$$\begin{aligned}\frac{d}{dt}X_{\text{ros}} &= -5Y_{\text{ros}} - 5Z_{\text{ros}}, \\ \frac{d}{dt}Y_{\text{ros}} &= 5X_{\text{ros}} + 5Y_{\text{ros}}/2, \\ \frac{d}{dt}Z_{\text{ros}} &= 10 + 5Z_{\text{ros}}(X_{\text{ros}} - 4),\end{aligned}\tag{16}$$

using a 4-th order Runge-Kutta integrator with time step  $\delta t = 10^{-3}$  from a random initial state. The coefficients of the Rössler system in Eq. (16) are chosen such that the system has a similar time scale to that of the Lorenz system. We then renormalize each of the three variables,  $X_{\text{ros}}$ ,  $Y_{\text{ros}}$ , and  $Z_{\text{ros}}$ , such that they all have a mean of zero and a variance of one. We then save the renormalized trajectory as the the Rössler-task input trajectory  $\mathbf{s}_{\text{ros}}(t)$  with time resolution  $\tau = 0.02$ .

**Avoiding overlapping attractors in multitask learning.** For the multitask learning cases depicted in both Fig. 3 and Fig. 4 in the main text, we further modify the input trajectories to prevent any overlap between the Lorenz attractor and the Rössler attractor by shifting the Lorenz-task input  $\mathbf{s}_{\text{lor}}(t)$  such that it has mean  $[10, 10, 10]$ , and by shifting the Rössler-task input  $\mathbf{s}_{\text{ros}}(t)$  such that it has mean  $[-10, -10, -10]$ .

## 4 The Recurrent Neural Network Model

In all of the systems that we instantiated *in silico*, we model the central system as a random recurrent neural network with  $N = 2000$  neurons,

$$\mathbf{f}(\mathbf{x}, \mathbf{s}) = \tanh(\mathbf{A}\mathbf{x} + \mathbf{W}_{\text{in}}\mathbf{s} + \mathbf{c}), \quad (17)$$

where  $\tanh(\cdot)$  operating on a vector returns a vector with the same shape that satisfies  $[\tanh(\mathbf{x})]_i = \tanh([\mathbf{x}]_i)$ . The adjacency matrix  $\mathbf{A} \in \mathbb{R}^{2000 \times 2000}$  is the weighted adjacency matrix of the recurrent neural network. The input weight matrix  $\mathbf{W}_{\text{in}} \in \mathbb{R}^{2000 \times 3}$  propagates the 3 input variables to the 2000 neurons. The vector  $\mathbf{c} \in \mathbb{R}^{2000 \times 1}$  is a random vector with its elements drawn uniformly from  $[-1, 1]$ . We choose a simple topology of the recurrent neural network where the adjacency matrix  $\mathbf{A}$  is a sparse Erdős-Rényi random matrix. The sparseness of  $\mathbf{A}$  (the fraction of non-zero elements) is set to be 0.02. All non-zero elements in  $\mathbf{A}$  are drawn uniformly from  $[-\sigma, \sigma]$ . The value of  $\sigma$  is determined by having the spectral radius of  $\mathbf{A}$  (the magnitude of the largest eigenvalue of  $\mathbf{A}$ ) to be 1.4. We construct the input weight matrix  $\mathbf{W}_{\text{in}}$  in such a way as to ensure that each neuron receives one and only one input variable from the 3-dimensional input. The input connection strength (each nonzero element in  $\mathbf{W}_{\text{in}}$ ) is drawn uniformly at random from the interval  $[-0.05, 0.05]$ .

## 5 Learning by Adapting the Output Weight Matrices

Throughout the examples given in the main text, exemplary Lorenz and Rössler input trajectories all have length 1000 time units ( $5 \times 10^4$  data points based on the sampling rate  $\Delta t = 0.02$ ). During

each learning phase, the output matrix  $\mathbf{W}_{\text{out}}$  adapts accordingly following

$$\mathbf{W}_{\text{out}}(t + 1) = \mathbf{W}_{\text{out}}(t) + \alpha \Delta(t) \mathbf{x}(t), \quad (18)$$

where  $\alpha$  is the learning rate. Notice that there is a transient period from the initial central system state  $\mathbf{x}(0)$  before the generalized synchronization occurs. We thus freeze  $\mathbf{W}_{\text{out}}(t)$  for time points  $0 \leq t \leq 5000$  during each learning phase. We let the system learn each task 1000 times. For cases where the RNN is asked to learn both the the Lorenz task and the Rössler task (Figs. 3 and 4 in the main text), we let it learn both tasks in an alternate manner. To ensure that  $\mathbf{W}_{\text{out}}$  converges, we empirically choose the learning rate  $\alpha = 10^{-3}$  for the first 300 repetitions and then decrease the learning rate afterward so that the later adaptations can fine-tune  $\mathbf{W}_{\text{out}}$ .

## 6 Comparison with Previous Work

Previous studies have demonstrated that recurrent neural networks can be trained to accomplish many tasks. For example, reservoir computing networks are trained to generate periodic patterns<sup>21</sup> and even to replicate long-term dynamics on a chaotic attractor.<sup>21,22,56</sup> Our structural learning framework incorporates the idea that a recurrent neural network learns the chaotic dynamics by reconstructing the chaotic attractor.<sup>57</sup> Using this framework, we show that the system has the ability to adaptively learn dynamics on multiple chaotic attractors. A complementary adaptive learning scheme called “FOLLOW” shows that a recurrent spiking neural network can learn nonlinear dynamics by adjusting the synapses between neurons.<sup>16</sup> A unique feature of our model is that the recurrent network and the synapses that comprise it are kept fixed such that different external inputs drive the dynamics of the RNN. We made this choice because it allows for an easy implementa-

tion and interpretation of the learning of more than one chaotic attractor. In fact, the adaptation of the internal output connections also allows the learning of other downstream functions (such as separating mixed input) without adversely affecting the perception manifold.